MECHANICAL EVALUATION OF A RESPIRATORY DEVICE

Lutero Carmo de Lima
João Manoel Dias Pimenta
João Batista Furlan Duarte
Universidade de Fortaleza, Centro de Ciências Tecnológicas – 60811-905 – Fortaleza – CE - Brazil
luterocl@unifor.br

Francisco Paula Lépore Neto
Universidade Federal de Uberlândia, Departamento de Engenharia Mecânica – 38400-902 – Uberlândia – MG – Brazil

Paulo Toshio Abe
Fundação Estadual de Lavras, Departamento de Fisioterapia – 37200-000 – Lavras – MG - Brazil
toshio@lavras.br

Abstract. *The objective of the present article is to mechanically characterize the behavior of the Flutter VRP$_1$, a respiratory physiotherapy device. The device basically resembles a smoke-pipe with a conical cavity where a stainless steel sphere is located and which floats up and down due to the intermittent air flow of patients. The sphere maintains an oscillatory movement whose frequency is function of the air flow and orientation of the device. The oscillatory frequency of the sphere inside the Flutter when matched with the natural frequency of the thoracic chest of the patient will produce the effect of resonance which by its turn will move the pulmonary secretions. A numerical formulation was made and an experimental set up was assembled in order to study the oscillatory frequency of the sphere under different conditions of air flow, fluid pressure, device orientations and sphere's materials and weights. Interesting results presented by this article point to the mechanical optimization of the device and show information that certainly will be beneficial to the professionals of the respiratory physiotherapy.*

Keywords. *oscillatory frequency, floating sphere, respiratory physiotherapy, Flutter VRP$_1$.*

1. Introduction

The VRP1-Desitin® device, also known as Flutter, is a small pocket device designed for the treatment of patients suffering from chronic mucus retention and bronchial collapse. Although being simple in its design, the Flutter has been showing encouraging performance when compared to traditional respiratory physiotherapy such as, for example, autogenic drainage (LINDEMANN, 1992). It is based on oscillations of air in the respiratory tract during expiration. Pressure and flow variations depend on the position of the mouthpiece and effort of breathing.

As shown in Figure 1, the Flutter is constituted of a mouthpiece (a), a hard material cone (b), a 28 grams high-density stainless steel sphere (c), and a perforated and removable lid (d).

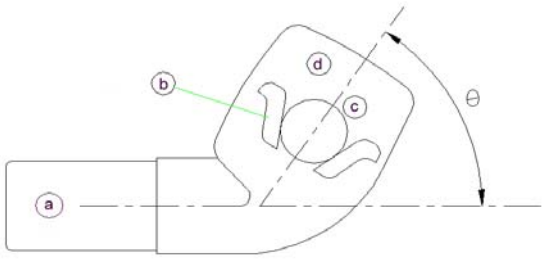

Figure 1. The Flutter device.

It works as follow. Before expiration the sphere closes the conical channel. During expiration, the instantaneous position of the sphere is resulted from the equilibrium state of its own weight, the cone angle and the pressure of the expired air. After the increase in the pressure, the sphere starts to move, permitting air to flow through the variable area orifice (the expiratory flow in this state is under strong acceleration). After this air pressure falls, the sphere rolls back to its initial position and it blocks the orifice, resulting again in the increase of the pressure. This process stimulates "bronchial percussion" easing the elimination of mucus and saliva and the frequency of this cycle can be adapted to each patient. The oscillation frequency, the air pressure and flow depend on the angle position of the mouthpiece and lid of the device as well on the expiration effort.

The device was submitted to two kinds of evaluation. The first one was the formulation of a numerical model of the flow through the Flutter using the finite element Computational Fluid Dynamics (CFD) ANSYS 5.2^{TM} code, in order to calculate the aerodynamic force acting on the sphere. The second one was the experimental observation of the behavior

of the Flutter through the measurements of the sphere vibratory motions inside the lid, the airflow rate, the inlet pressure, and its behavior with spheres of different materials other than steel such as aluminum, tecnew and teflon.

2. Mathematical and Computational Model

The Flutter computational model was built using the finite element method to simulate the steady state flow developed at the inlet and outlet ducts and at the region around the sphere. The fluid is the air with physical properties independent of the temperature. The package ANSYS 5.2 through its module of Computational Fluid Dynamics named FLOTRAN was used, considering the K - ε model of turbulence, developed by LAUNDER and SPALDING (1974). The elements are quadrilateral (FLUID171) and the model is axisymetric in the flow direction X. The mesh is refined at the central region of the model, where the sphere is close to the conical wall, in order to achieve numerical convergence of the solution, after 60 iterations. The Figure 2 shows part of the mesh pattern at the central region of the model, and Figure 3 gives details of the mesh refinement near the sphere surface that is close to the conical wall.

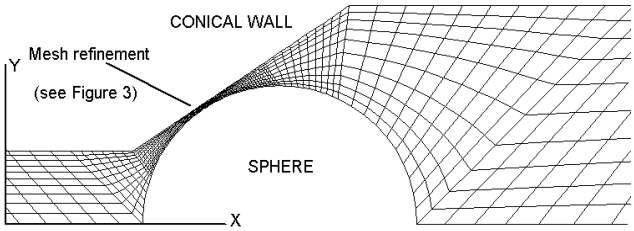

Figure 2. Part of the finite element model: mesh at central region.

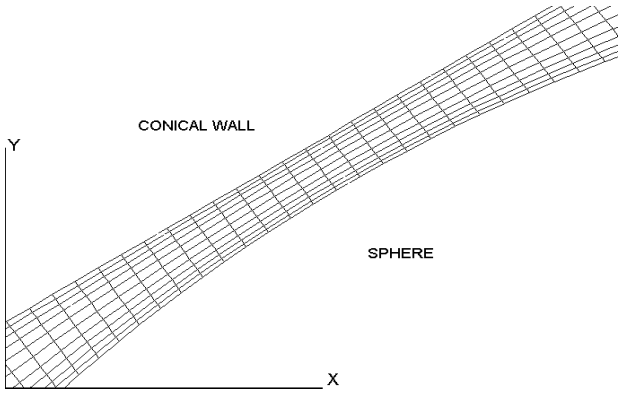

Figure 3. Finite element model: mesh refinement.

The applied boundary conditions impose zero velocities at the inner walls and at the sphere surface. The velocity in the Y direction is considered equal to zero on the axisymetric axis. To simulate a 2.0 m^3/h flow, the inlet velocity in the X direction is V_{in} = 7.13 m/s. At the outlet, the atmospheric pressure is imposed. Statically positioning the sphere at 23 different locations on the X direction, the velocity field and the pressure distribution were determined. The Figures 4, 5 and 6 show the results of the velocity field and pressure distribution for some of the simulated sphere positions. Only half of the cross-longitudinal section grid of the Flutter is shown, considering that X is horizontal and the position x = 0 corresponds to the condition of flow obstructed by the sphere.

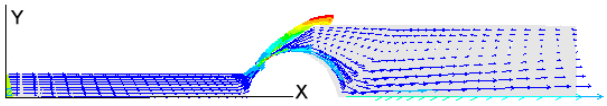

Figure 4. Velocity field: complete model for V_{in} = 7.13 m/s and position x = 0.5736 mm.

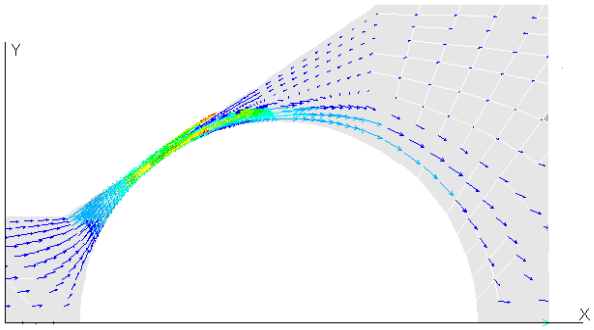

Figure 5. Velocity field: region around the sphere, for V_{in}=7.13 m/s and sphere position x = 0.5736 mm.

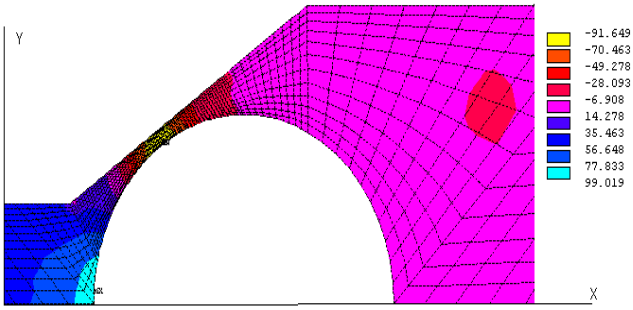

Figure 6. Pressure distribution (x 100 Pa) on the central region of the model, for V_{in} = 7.13 m/s and sphere position x = 1.3736 mm.

The pressure distribution at the model central region is shown, for the same conditions of Figure 6, but for a sphere position x = 1.3736 mm, which corresponds to a greater orifice area. The maximum pressure of 9902 Pa is in front of the sphere. The pressure is negative at the region where the sphere is close to the conical wall. A vortex formation is present at the right side of the sphere, what can be verified by the pressure negative value of –2000 Pa. This effect can also be observed in the velocity vectors distribution shown in Figure 4, although the airflow rate for this situation is relatively small.

The pressure distribution on the sphere is obtained by selecting the model nodes on its surface. The Figure 7 shows one of these distributions. The frontal position is at the left side, where the angular position θ is 0 degrees.

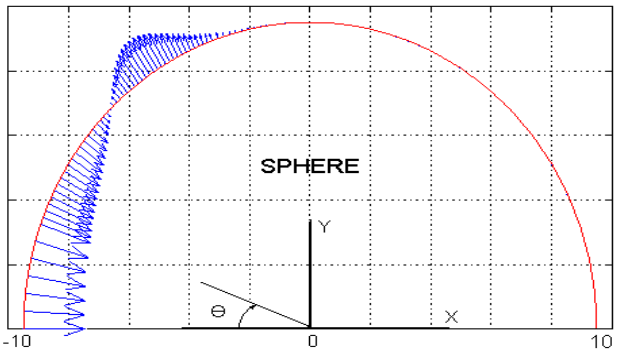

Figure 7. Pressure distribution on the sphere P(q), for V_{in} = 7.13 m/s and sphere position x = 0.5736 mm.

The lift forces acting on the sphere are calculated by integrating the pressure distributions obtained for each sphere position x, varying from 0.1736 to 2.5 mm, at steps equal to 0.1 mm. In Figure 8, the solid line is the mathematical function fitted to the numerical data by a least square procedure, with mean error of 1.342. 10^{-5}. When x is less than 0.1736 mm, the finite element model does not converge because the element geometry is strongly distorted, increasing the numerical errors.

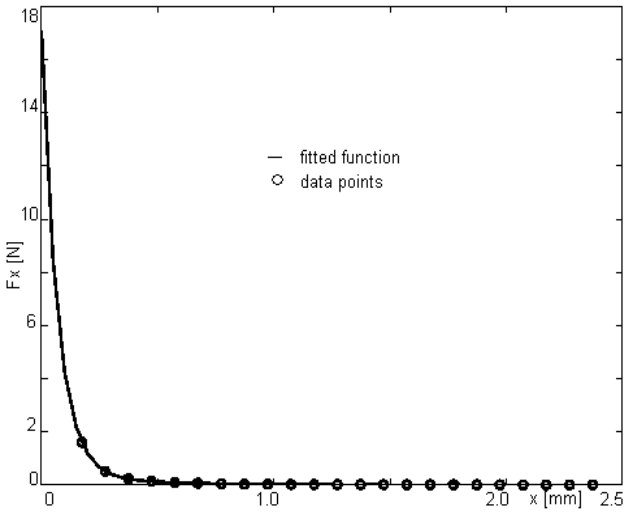

Figure 8. Lift force as a function of the sphere position for V_{in} = 7.13 m/s.

A further refinement of the mesh is not computationally feasible because of the amount of computer memory available and also the processing time involved to obtain the solution. So, the lift aerodynamic force model can not be used to calculate the sphere vibrations for displacements less than 0.1736 mm, but this model can be used to extrapolate force values for x greater than 2.5 mm, considering that F(x) has a smooth variation for greater values of x

To evaluate the vibratory motion of the sphere a simplified one degree of freedom dynamic model was assumed, as shown in Figure 9, where the X direction is vertical. The forces acting on the sphere are the aerodynamic, F(x), and the gravitational, mg.

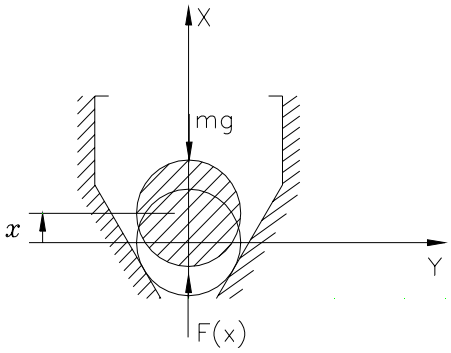

Figure 9. Dynamic model of the Flutter's lid in the vertical position

The mathematical model is presented in Equation 1, where m is the sphere mass, g is the acceleration of gravity, and F(x) is the nonlinear aerodynamic lift force.

$$m\ddot{x} = F(x) - mg \tag{1a}$$

$$F(x) = c_1 e^{-\lambda_1 x} + c_2 e^{-\lambda_2 x} \tag{1b}$$

For V_{in} = 7.13 m/s, the function that describes F(x), as shown in Figure 8, has the following parameters: c_1 = 16.635 N, c_2 = 0.473 N, λ_1 = 14573 m^{-1} and λ_2 = 3054 m^{-1}. Equation 1 is solved numerically by a 4th order Runge-Kutta method, using a time step dt = 0.5 ms. The steady state vibratory motion, is shown in Figure 10 where only the last 2048 data points are plotted.

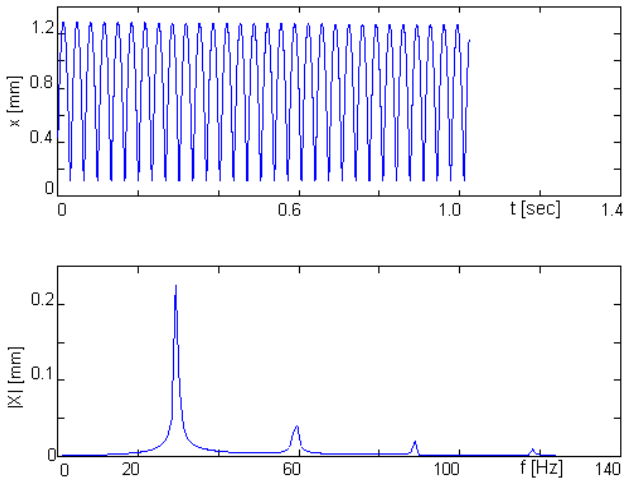

Figure 10. Dynamic model simulation results: x(t) and |X(f)| for V_{in} = 7.13 m/s.

For this simulation, the sphere displacement has a mean value equal to 0.625 mm and maximum value of 4.72 mm that occurs just at the beginning of the sphere transient motion. The time domain signal x(t) has periodic characteristic and the velocity presents strong variations when the sphere is almost obstructing the flow. This behavior is in accordance with the fact that the aerodynamic lift force in that position is maximum and decreases exponentially with x. The spectrum has resolution df = 0.9765 Hz and shows a fundamental frequency fp = 29.3 Hz and its higher harmonics.

3. Experimental Procedure

The experimental set up is shown in Figure 11. A mechanical compressor feeds air to the Flutter. An inductive proximity transducer, which is linked to a signal conditioner system, measures the vertical movement of the sphere. The proximity transducer has a global static sensitivity of 2.156 V/mm and a 2.5 mm full scale. Air pressure is measured by a piezoelectric transducer which is coupled to a 500 gain voltage amplifier and has static sensitivity of 9167 Pa/V. The airflow rate at the entrance of the Flutter is measured by a calibrated rotameter with the operation range between 1.5 and 16 m^3/h. The airflow rates are controlled by a valve. A Signal Analyzer acquires time signals of the sphere position and pressure at the entrance tube of the Flutter and the digitized data is subsequently transferred to a microcomputer. In other situation, airflow rates and inlet pressure were measured when the mouthpiece of the Flutter was in 0°, +30° and –30° orientations.

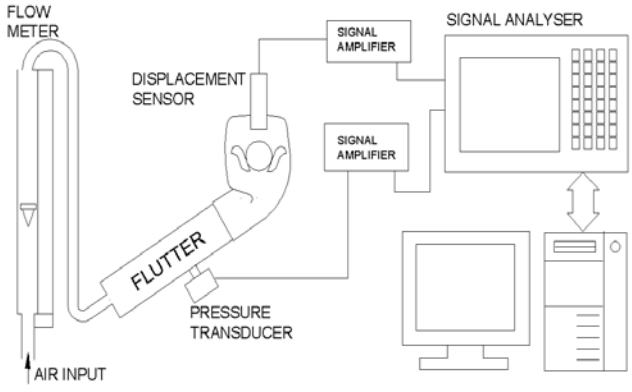

Figure 11. Experimental set-up and measurement system.

As can be seen in Figure 12 there were manufactured spheres of aluminum, tecnew and teflon with nominal diameter of 20mm which is basically the same as the diameter of the original sphere of stainless steel. The measured mass of the stainless steel sphere was of 27.88 grams, 9.7 grams for the sphere of aluminum, 4.16 grams for the sphere of tecnew and 4.98 grams for the sphere of teflon.

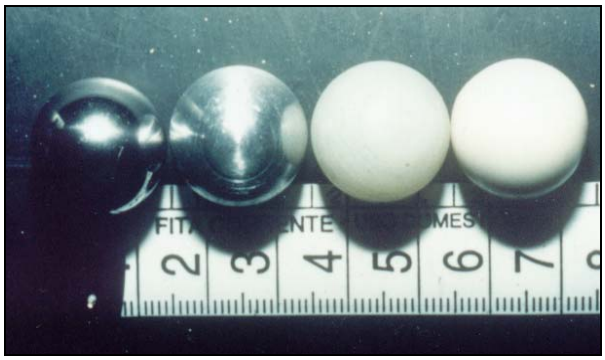

Figure 12. Spheres of stainless steel, aluminum, tecnew and teflon (respectively from left).

4. Results

Experiments were made with airflow rates, Q, ranging between 2 and 8 m^3/h, which is the range of airflow rate that a human being is able to produce. The entrance tubing (mouthpiece) in the Flutter makes a 30^o angle with respect to the horizontal direction, so that the air outlet tube, which contains the conical section and the sphere, keeps the vertical position.

The Figures from 13 up to 17 show experimental results on the measurements of the sphere vertical vibration and the pressure inside the entrance tubing, for airflow rates from 2.0 up to 7.8 m^3/h.

The time signals represent a single sample and all the spectra results were obtained from an average procedure of 10 samples.

As can be seen in Figures 13 and 14, for Q = 2.0 m^3/h, the time and frequency domain signals of displacement and pressure present a periodic nature which is apparent by the existence of a fundamental frequency and its higher order harmonics. (BENDAT & PEARSOL, 1986).

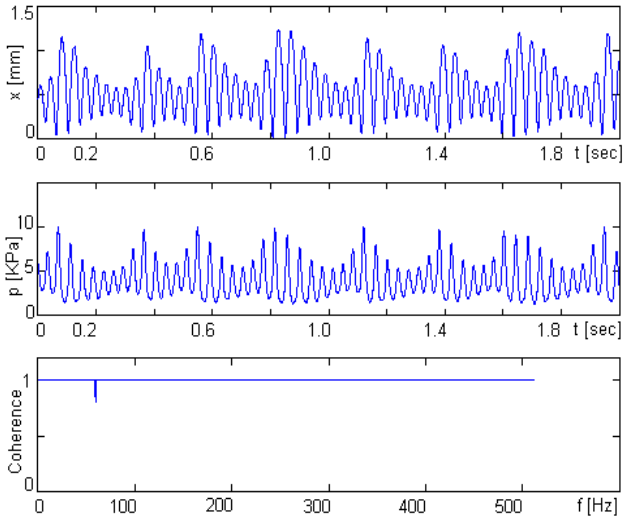

Figure 13. Displacement x(t), input pressure p(t) and coherence function for Q = 2.0 m^3/h.

The spectra of the signals obtained for Q = 2.0 m^3/h, are shown in Figure 14, where the highest peak is the fundamental frequency and the lower ones present a frequency spacing of 4.125 Hz. The presence of side bands in the displacement and pressure spectra indicates modulation in amplitude.

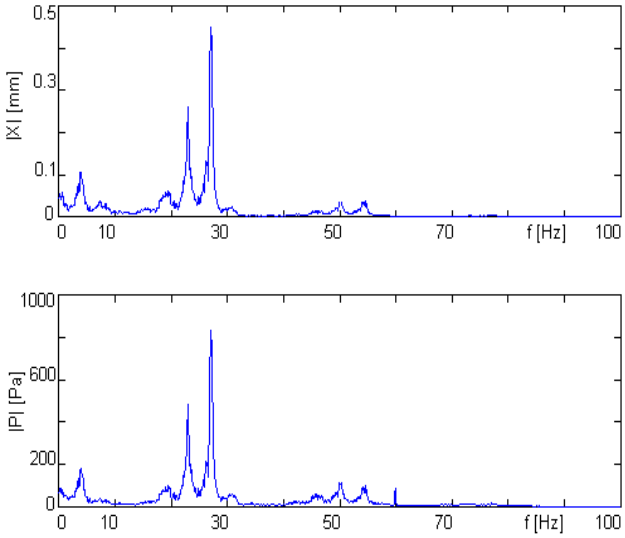

Figure 14. Spectra |X(f)| and |P(f)|, for Q = 2.0 m^3/h

The coherence function $\gamma^2_{xp}(f)$, resulted almost equal to unity for the analyzed frequency band (0 - 500 Hz). The only value less than unity indicates the presence of an electromagnetic interference at f = 60 Hz.

The correlation between the displacement and pressure signals can be observed in the following figure. The Figure 15a shows, for Q = 2.0 m^3/h, the spectra |X| and |P|, normalized, respectively, by their maximum values. A constant value of 0.1 units was added to |P| artificially separate the two curves, since they are practically coincident, The Figure 15b shows similar results, measured for Q = 7.8 m^3/h.

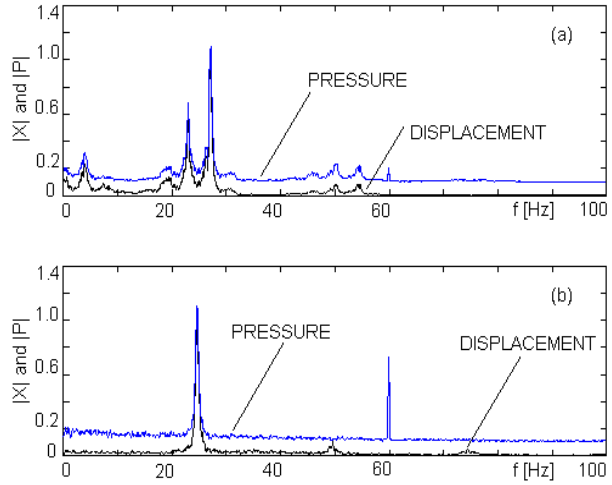

Figure 15. Pressure |X(f)| and displacement |P(f)| spectra, for Q = 2.0 m^3/h in (a), and Q= 7.8 m^3/h in (b).

The results in Figure 15 were obtained for the two extreme values of the input flow rate. It can be observed that, despite the strong non-linearity of the lift aerodynamic force that acts on the sphere, the displacement and the inlet pressure spectra follow the same pattern. The greater differences occur for Q = 7.8 m^3/h, in Figure 15b. The peaks at the second and third harmonics of the displacement signal are not present in the pressure signal. The large peak of the pressure signal at 60 Hz represents the influence of an electromagnetic noise caused by the main supply, and it is not related to the sphere vibration

Considering that the coherence of x(t) and p(t) is equal to one in the frequency band 0 – 500 Hz, the sphere vibratory motion is fundamentally excited by the pressure fluctuation and vice versa.

The fundamental or carrier frequency and its lateral frequency bands vary with the imposed air flow rate in the entrance of the Flutter.

In the time domain, for airflow rates less than 5 m^3/h, a strong modulation in amplitude on the sphere vibration and on the pressure signals was observed.

The intensity of the modulation keeps falling until an airflow rate of 6 m^3/h, and after that, it practically disappears, indicating a transition on the behavior of the dynamic system. On the frequency spectra of the inlet pressure, this modulation can be confirmed by the presence of lateral bands around the fundamental frequency and its harmonics, as

can be seen in Figure 16. The modulation effect for Q = 3.8 m^3/h is larger than for Q =6.0 m^3/h, which can be observed on the time and on the frequency domain signals.

Similar behavior is found in the sphere displacement signals, as shown in Figure 17, for the same values of the air input flow rate.

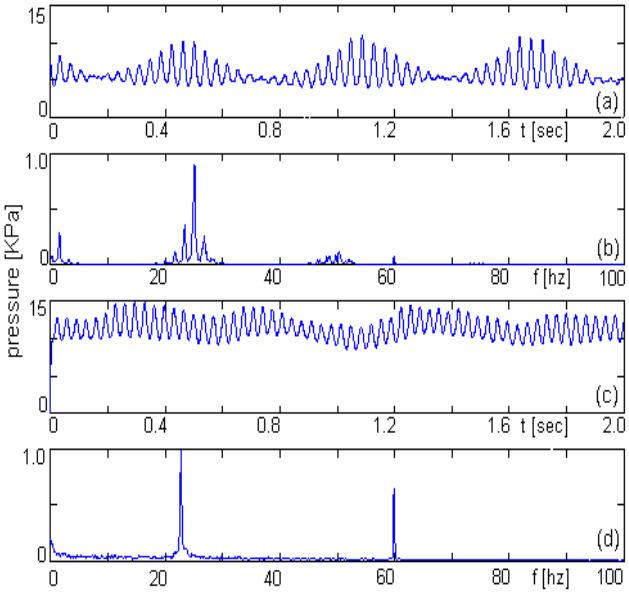

Figure 16. Comparison of the pressure signals p(t) and |P(f)|, for Q = 3.8 m^3/h in (a), (b) and for Q = 6.0 m^3/h in (c) , (d).

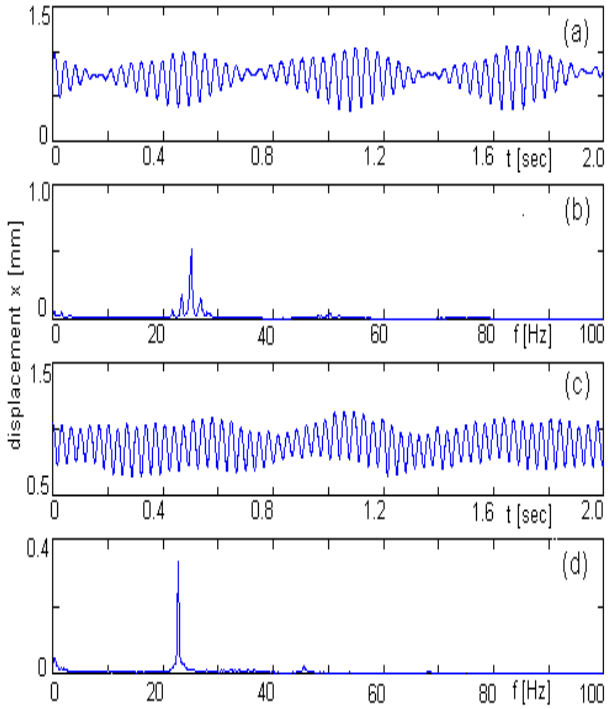

Figure 17. Comparison of the displacement signals x(t) and |X(f)| for Q = 3.8 m^3/h in (a) , (b) and for Q = 6.0 m^3/h in (c) , (d).

The modulation can be calculated by measuring the frequency spacing of the lateral spectrum lines that are located around the fundamental frequency peaks. These side bands are also present around the higher harmonics of the fundamental frequency, but with smaller amplitudes. The periodicities of the pressure and displacement spectra, were calculated through the complex spectrum transform, and resulted identical.

According to Table 1, a small reduction in the fundamental frequency (fp) and in the modulation frequency (Bf) with the increase in the airflow rate, can be observed.

For Q values greater than 6.0 m^3/h, the amplitude modulation effects are not present either on the pressure or on the displacement signals.

Table 1. Fundamental frequency and the lateral bands spacing as function of airflow rate.

Q [m^3/h]	2.0	3.0	3.8	5.0	6.0	7.8
Fp [Hz]	27.13	27.25	25.13	25.38	22.8	24.5
Bf [Hz]	4.13	3.63	1.75	1.50	1.02	-o-

A visual observation of the sphere did show that for higher airflow rates its movement is basically vertical and there is no occurrence of shocks of the sphere with the conical wall of the Flutter. In other situations, mainly for lower flow rates, between 2.0 and 3.8 m^3/h, the sphere rotates and translates in the vertical and horizontal directions, touching the conical wall, promoting the existence of the low frequency modulation on the sphere vibration. This behavior was not considered in the present computational model and this hinders its confirmations on the simulation results.

Other preliminary experiments were conducted, changing the orientation of the inlet tubing. For these situations the sphere motions are similar to those obtained for low flow rates. Even using the maximum flow rate that can be supplied by the feeding compressor, it was not possible to achieve the stabilization of the sphere vibrations. The cause of this behavior can be explained by the constant presence of shocks of the sphere against the conical wall.

In Figure 18 it is shown adjusted curves of air flow rates against pressure inside the Flutter's mouthpiece in the 0^o position. Every curve is derived from experimental measurement for each sphere. As can be observed, spheres of tecnew and Teflon did show a level of pressure 25% lower than the level presented by the sphere manufactured of steel.

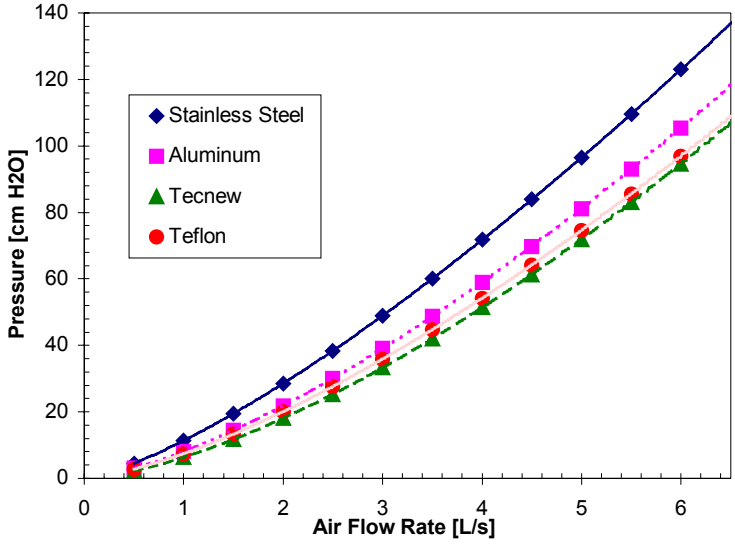

Figure 18. Adjusted curves of air flow rate x pressure for different spheres with Flutter in the 0^o position.

Figure 19 shows curves of airflow rates against pressure inside the Flutter's mouthpiece in the $+30^o$ position. For this position, spheres of aluminum, tecnew and Teflon presented the same level of pressure against the considered range of airflow rates. They presented basically a level of pressure 35% lower than the corresponding level of the original sphere.

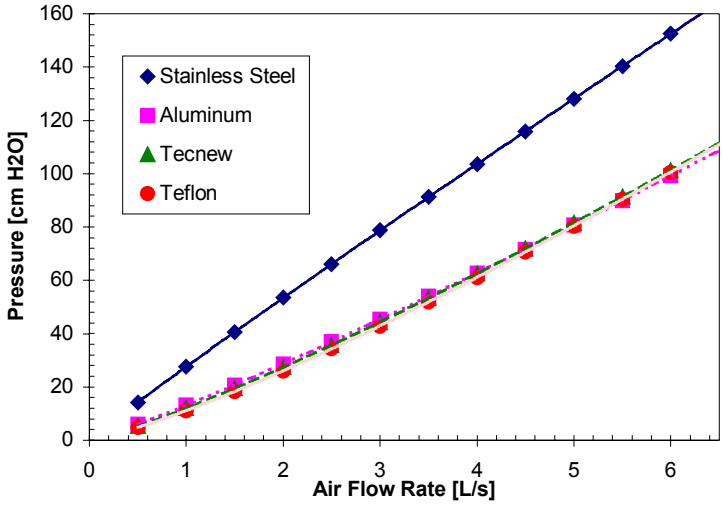

Figure 19. Adjusted curves of air flow rate x pressure for different spheres with Flutter in the +30° position.

Figure 20 shows curves of airflow rates against pressure inside the Flutter's mouthpiece in the –30° position. For this position every sphere presented practically the same level of pressure for the considered range of airflow rates.

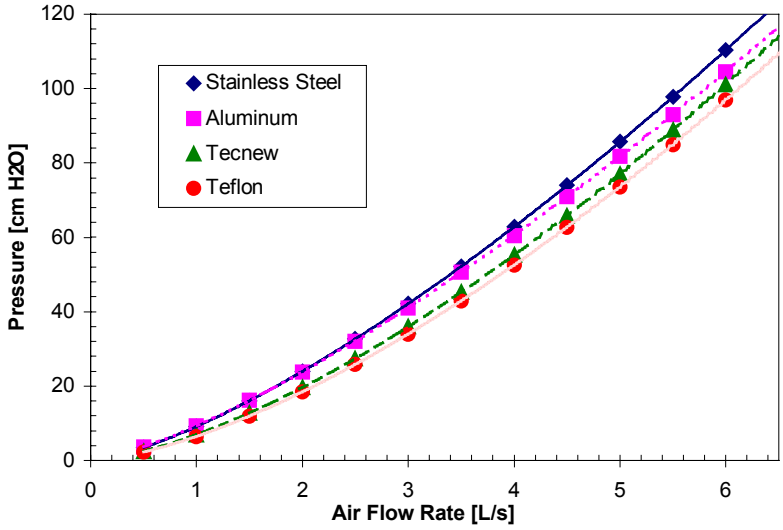

Figure 20. Adjusted curves of air flow rate x pressure for different spheres with Flutter in the -30° position.

5. Discussion of Results

The dynamic behavior of the Flutter device, used for respiratory physiotherapy, was dynamically investigated. Based on a theoretical modeling and on a numerical simulation, it was possible to study the influence of the air inflow velocity, on the aerodynamic lift force, on the vibration of the sphere, and on the inlet pressure fluctuations.

The finite element model mesh at the region where the sphere approaches the conical wall was refined to allow the calculation of the lifting aerodynamic force. In the present work, further mesh refinement was not possible considering the available computer hardware.

The proposed approach uses the finite element model static solution to evaluate the lift aerodynamic force at different sphere positions along the x direction. The fitted non-linear force function is used as an excitation of the dynamic equilibrium of the sphere. This formulation assumes that the airflow rate is invariant with the sphere vibratory motions.

The finite element model cannot handle with sphere positions lower then x = 0.1736 mm. To overcome this difficulty the lift force was analytically calculated for the position x = 0, where the sphere blocks the input air flow. The value of F(0) was included in the simulated lift force data set used to obtain the fitted function F(x), presented by equation 1, and shown in Figure 8.

The flow rate Q = 2.0 m^3/h was used to compare the experimental results with those obtained by the adopted computational model.

In this situation, the sphere displacement mean values and their variation ranges are equal to 0.62: (0.18 – 1.3) mm for the simulated case, and 0.56: (0.06 – 1.24) mm, for the experimental test, corresponding to a +10.7% difference.

The simulated and experimental fundamental frequencies are equal to 29.30 Hz and 27.12 Hz, corresponding to a difference of 8 %.

Despite these acceptable errors, it is not possible to extend, at the present stage of this research, the application of the computational model for other Flutter orientations than 0 degrees with respect to the horizontal direction, until a new computational model were developed.

The computational model did not detect the side band spectral amplitudes associated to the amplitude modulation effect. This simplified dynamic model can not handle either the sphere lateral and rolling motions and or the sphere impacts on the surface of the conical wall, which are important effects observed in the experiments.

To improve the computational model, besides the mesh refinement as mentioned earlier, it will be necessary to consider the sphere motions in tree dimensions, and the shocks between the sphere and the conical wall. Using an unsymmetrical 3-D finite element model and a coupled field transient analysis this can be done. The computational code ANSYS 5.2™, can be used to solve this problem, including structural contact elements to represent the shock between the sphere and the conical wall.

Another possible approach uses the Chimera grid formulation for the solution of fluid flow around flexible structures, by overlapping the fluid and the solid body meshes, and constructing an interpolating interface. This technique was presented by MEAKIN (1993), HOLST (1995), and PETERSSON (1999).

The experimental set-up furnished displacement and pressure time signals. The system characteristic frequencies could be easily determined by analyzing the signals in the frequency domain. The cepstrum is an important technique to evaluate the amplitude modulation effects associated with the dynamical behavior of system.

For the situation where the mouthpiece of the Flutter was kept horizontal, the results demonstrated that the sphere displacement fundamental oscillation frequency and its harmonics can be changed by the input airflow rate, as presented in Table 1.

The experiments have shown that only for flow rate values up to 5.0 m^3/h, the modulation intensity is significant, indicating that greater flow rates may not produce the desired effect on the patient.

Although the Flutter has been used in almost every country of the world as a successful alternative for the traditional respiratory physiotherapies mainly due to its design, easy to use, efficiency and cost competitive, only Lindemann (1992) experimentally verified that the level of pressure inside that device can reach 75 cm H2O if the patient is blowing it at the horizontal orientation of the mouthpiece in a expiration air flow rate of 5 l/s which is not very demanding for a usual patient. After King et al. (l983) the necessary requisite for an effective mucus transport to the cephalic direction during the high frequency thoracic compression manouvre is the maintenance of limited range of air flow rate between l and 3 l/s. On the other hand the great majority of researchers (Chatam et al., 1993; Girardi and Terki, 1994; Hardy, 1994; Swift et al., 2000; Leru et al., 1994; Konstan et al., 1994; Newhouse et al., 1998; Bellone et al., 2000) on Flutter affirms that on that range of operation the Flutter shows level of pressure of 10 to 25 cm H2O. The fact is that the recommended range of air flow rate can be easily surpassed but on the other hand the level of pressure can reach value which if continued would conduct the patient to adverse reaction such as dizziness or pneumothorax if the patient presents some kind of precondition. Considering the air flow rate of 3 l/s, as can be seen in Figure 18, the pressure inside the Flutter operating at the horizontal position and with the stainless steel sphere will reach the value of 50 cm H2O and will reach 40 cm H2O for aluminum and 35 cm H2O for tecnew or teflon. The observed range of pressure of 10 to 25 cm H2O affirmed by the above referenced authors as for the case of the original sphere will limit the air flow rate to about 2 l/s and this limitation can be influential on the respiratory physiotherapy.

As for the case of utilization of the Flutter on $+30^o$ position which is a normally used practice because sometimes the patient is stimulated to that orientation of the Flutter in order to provocate the resonance that will displace the mucus, the level of pressure inside the device will reach 80 cm H2O for the case of the original sphere and 40 cm H2O for the case of the others spheres, as can be seen in the Figure 19. Even being intermittent that level of pressure (80 cm H2O) would be dangerous for some patients.

As for the case of utilization of the Flutter on the -30^o position as can be observed in the Figure 20 all spheres presented the same level of pressure (about 40 cm H2O) for the considered range of air flow rate.

The time domain signals of displacement and frequency shown in the Figure 17 for two air flow rates present a periodic nature which is apparent by the existence of a fundamental frequency and its higher order harmonics for the case of air flow rate of l.2 l/s and only a peak of frequency for the case of 1.8 l/s. The highest peak represents the fundamental frequency of the sphere inside the Flutter and the lower ones represent harmonics that by its turn present a frequency spacing indicating modulation of the displacement of the sphere by the air flow. The presence of the modulation is the necessary factor for the existence of the beneficial resonance. As can be observed in Figure 17 the modulation effect is more present for air flow rate lower than 2 l/s and after that value it practically disappear indicating a transition on the behaviour of the dynamics of the Flutter.A study of the effects of shock and vibration on the human body presented by Harris (1988) shows that the natural frequencies of the mouth-chest system fall in the 5 to 11 Hz

frequency band. These values were experimentally obtained by applying oscillating air pressure to the mouth and measuring the vibrations on the chest wall. The natural frequency values may vary and mainly depend on the seating or standing position of the human body. On the other hand, Cegla and Retzow (1993) reported that lung-chest natural frequencies might vary between 12 and 15 Hz. The comparison of the effects of high-frequency oral airway oscillations, high frequency chest wall oscillation and conventional chest physical therapy on weight of expectorated sputum in patients with stable cystic fibrosis was studied by Scherer et al. (1998). The tested frequencies in the airway method were 8 Hz and 14 Hz. The frequencies applied in the wall chest oscillations technique were 3 Hz and 16 Hz. For these two techniques the weight of expectorated sputum is higher for the low frequencies. When compared this information with the behavior of the present device it may be reasonable to stress that the effectiveness of the Flutter to improve sputum elimination in patients of the respiratory physiotherapy is eventually most present when the fundamental and the modulating frequencies of the inlet pressure have values close or multiple to some of the natural frequencies of the mouth-bronchi-lungs-thoracic cage system.

6. Conclusion

The present article studied the mechanical behavior the Flutter VRP1, a device used in the respiratory physiotherapy, and it may conclude that:

- the stainless steel original sphere inside the Flutter may produce high level of pressure (more than 80 cm H2O) in the bronchi-lungs system of a patient if the air flow rate is higher than 3 l/s;
- spheres manufactured of materials lighter than steel, as for example aluminum, tecnew or teflon effectively reduces the level of pressure inside the Flutter and depending on its orientation the reduction can reach till 50%;
- the beneficial effect of resonance for the displacement of mucus is limited to the range of air flow rate, that is, up to about 3 l/s.

7. References

Bellone, A., Lascioli, R., Raschi, L., Guzzi, L. and Adone, R., "Chest Physical Therapy in Patients with Acute Exacerbation of Chronic Bronchitis: Effectiveness of Three Methods", Arch. Phys. Med. Rehabil., v. 81, pp. 558-560, 2000.

Bendat, J.S. and Piersol, A., "Random Data Analysis and Measurement Procedures", John Wiley & Sons, 2nd Edition, ISBN 0 471 04000 2, 1986.

Cegla, U.H. and Retzow, A., "Physiotherapie mit dem VRP1 bei Cronisch Obstruktiven – atemwegserkrankungen: Ergebnisse einer Multizentrischen vegleichsstudie", Pneumologie, v. 47, pp. 636-639, 1993.

Chatham, K., Marshall, C., Campbell, I.A. and Prescott, R.J., "The Flutter VRP1 Device for Post-thoracotomy Patients", Physiotherapy, v. 79, pp. 95-98, 1993.

Girard, J.P. and Terki, N., 1994, "The Flutter VRP1: A New Personal Pocket Therapeutic Device Used as an Adjuct to Drug Therapy in the Management of Bronchial Asthma", J. Invest. Allergol. Clin. Immunol., v. 4, pp. 23-27, 1994.

Hardy, K., "A Review of Airway Clearance: New Techniques, Indications and Recommendations", Respiratory Care, v. 39, pp. 440-455, 1994.

Harris, C. M., "Shock and Vibration Handbook", McGraw-Hill, 3rd Edition, ISBN 0070268010, 1988.

Holst, T.L., " Numerical Solution of the full Potential Equation using a Chimera grid Approach", NASA Report TM-110360, 38 pp., Ames Research Center, Moffett Field, CA, USA, 1995.

King, M., Phillips, D.M., Gross, D., Vartian, V., Chang, H.K. and Zidulka, A., "Enhanced Tracheal Mucus Clearance with High Frequency Chest Wall Compression", Am. Rev. Respir. Dis., v. 128, pp. 511-515, 1983.

Konstan, M.W., Stern, R.C. and Doershuk, C.F., "Efficacy of the Flutter Device for Airway Mucus Clearance in Patients with Cystic Fibrosis", J. Pediatr., v. 124, pp. 689-693, 1994.

Launder, B.E. and Spalding, D.B., 1974, "The Numerical Computation of Turbulent Flows, Computer Methods in Applied Mechanics and Engineering, vol. 46, pp. 269-289, 1974.

Lépore Neto, F.P., De Lima, L.C. and Gastaldi, A.C., "Dynamic Behaviour of a Respiratory Physiotherapy Device", Revista Ciência e Engenharia, v. 9/1, pp. 62-67, 2000.

Leru, P., Bistriceanu, G., Ibraim, E. and Stoicescu, P., "Flutter VRP1 Desitin – A New Physiotherapeutic Device for the Treatment of Chronic Obstructive Bronchitis", Rev. Roum. Méd. Int., v. 32, pp. 315-320, 1994.

Lindemann, H., "Zum Stellenwert der Physiotherapie mit dem VRP1 – Desitin (Flutter)", Pneumologie, v. 46, pp. 626-630, 1992.

Meakin, R., "Moving Body Overset Grid Methods for Complete Aircraft Tiltrotor Simulations, AIAA Computational Fluid Dynamics Conference, pp. 576-588, Orlando, FL, USA, 1993.

Newhouse P.A., White, F., Marks, J.H. and Homnick, D.N., "The Intrapulmonary Percussive Ventilator and Flutter Device Compared to Standard Chest Physiotherapy in Patients with Cystic Fibrosis", Clin. Pediatr. v. 37, pp. 427-432, 1998.

Petersson, N., "Na Algorithm for Assembling overlapping grid systems", SIAM J. Sci. Comput., vol. 20, nr. 6, pp. 1995-2022, 1999.

Scherer, T.A, Barandun, J., Martinez, E., Wanner, A. and Rubin, E.M., "Effect of High Frequency Oral Airway and Chest Wall Oscillation and Conventional Chest Physical Therapy on Expectoration of Patients with Stable Cystic Fibrosis", v. 113, pp. 1019-1027, 1998.

Swift, G.L., Rainer, T., Saran, R., Campbell, I.A. and Prescott, R.J., "Use of Flutter VRP1 in the Management of Patients with Steroid-dependent Asthma", Respiration, v. 61, pp. 126-129, 1994.